THE JOURNAL OF PHYSICAL CHEMISTRY C

Article

pubs.acs.org/JPCC

Comparing van der Waals Density Functionals for CO_2 Adsorption in Metal Organic Frameworks

Malay Kumar Rana, Hyun Seung Koh, Jinhyung Hwang, and Donald J. Siegel*

Mechanical Engineering Department, University of Michigan, Ann Arbor, Michigan 48109-2125, United States

Supporting Information

ABSTRACT: The accuracy of five recently proposed van der Waals (vdW) density functionals (optB86b, optB88, optPBE, revPBE, and rPW86), the semiempirical vdW method of Grimme (DFT-D2), and conventional local (LDA) and gradient-corrected (GGA-PBE) density functionals are assessed with respect to experimental enthalpies (ΔH) for CO_2 adsorption in four prototypical metal organic frameworks (MOFs) containing coordinatively unsaturated metal sites: M/DOBDC (M = Mg, Ni, and Co) and Cu-HKUST-1. Although the LDA and GGA functionals partially capture trends, they significantly overbind (LDA) and underbind (GGA) CO_2 with respect to the experimental enthalpies. The addition of a semiempirical r^{-6} dispersion term to the GGA exchange-correlation energy using "off the shelf" DFT-D2 parameters results in a substantial improvement both in trends and in the magnitude of the adsorption enthalpies. However, on average this approach still underbinds CO_2 as compared to the experimental data by ~7 kJ/mol (18%). Better accuracy is obtained with some of the nonempirical vdW density functionals, with the revPBE-based functional of Dion et al. [*Phys. Rev. Lett.* **2004**, *92*, 246401] yielding an average error of only ~2 kJ/mol (4%) relative to experiment. This improvement in energetics is accompanied by a slight decrease in the accuracy of predicted structures, as the revPBE functional overestimates the metal−CO_2 bond length by about 10%. The identification of an efficient vdW density functional capable of predicting the thermodynamics of CO_2 adsorption will facilitate rapid computational screening for optimal CO_2 adsorbents.

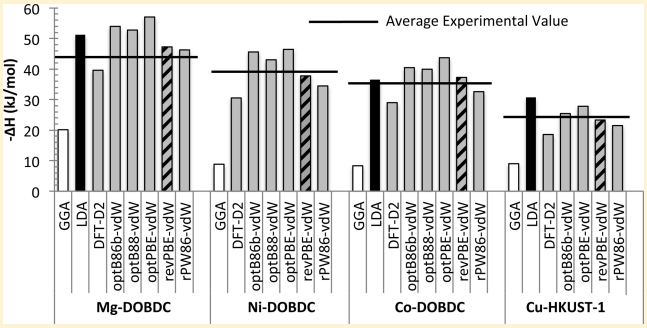

INTRODUCTION

Anthropogenic greenhouse gas (GHG) emissions are a major contributor to global climate change.[1] Although several compounds (CH_4, N_2O, etc.) have been implicated, carbon dioxide (CO_2) is by far the largest contributor.[1] The magnitude and growth rate of CO_2 emissions can be directly traced to fossil fuel use.[1] In the U.S., approximately 85% of the energy consumed comes from fossil fuels,[2] as does a similar fraction of energy used globally.[3] Population growth and economic development are expected to result in significant increases in CO_2 emissions: the U.S. Energy Information Administration has estimated that domestic consumption of fossil fuels will grow by 27% by the year 2030, resulting in a 33% increase in CO_2 emissions per year.[4]

Given its abundance and low cost, coal has become a cornerstone fuel for power generation.[5] A major drawback of coal combustion, however, is its high carbon intensity.[5] Because coal combustion will likely remain a significant power source for the foreseeable future, technologies capable of reducing its carbon intensity are of immense value.

One approach to reducing the GHG emissions of coal-fired power plants is carbon capture and sequestration (CCS).[6,7] State of the art approaches to CO_2 capture rely on the chemisorption of CO_2 by amine functional groups. While this approach can capture a large fraction of the CO_2 effluent,[8] the CO_2 absorption process is characterized by a large (~80−110 kJ/mol) exothermic heat of absorption,[9,10] resulting in significant energy requirements for solvent regeneration. These parasitics, and the associated problem of solvent degradation at high regeneration temperatures, consume up to ~30% of power output and increase the cost of electricity by ~80%.[11] For comparison, the U.S. Department of Energy has established a goal of 90% CO_2 capture with an increased cost of electricity of no more than 20%.[6]

Given their potential for facile regeneration, physisorptive materials (i.e., adsorbents)[12,13] are an attractive alternative to approaches that use chemisorptive interactions to capture CO_2. While many types of adsorbents are known,[13] metal−organic frameworks (MOFs)[14−19] are among the most promising candidates. MOFs are porous materials constructed from metal ions or polynuclear metal clusters assembled in a periodic fashion through coordination to organic linkers. The large number of possible clusters and linkers allows for a tunable "building-block" approach to their synthesis, resulting in a wide variety of MOF structures and compositions;[20−22] thousands of MOFs have been synthesized,[23] and more than 10^5 hypo-

Received: February 1, 2012
Revised: July 13, 2012
Published: July 18, 2012

   dx.doi.org/10.1021/jp3051164 | *J. Phys. Chem. C* 2012, 116, 16957−16968

thetical structures have been proposed.[22] MOFs hold the record for surface area, with some compounds exhibiting surface areas greater than 5000 m^2/g.[24−27] Although MOFs are a relatively new class of materials, they have already surpassed the performance of ultrahigh surface area carbons, which had previously defined the limits of CO_2 capacity at high pressures.[25] For example, Caskey et al.[20] have demonstrated that the MOF Mg/DOBDC exhibits the largest CO_2 uptake of any adsorbent at 1 bar.

The large number of MOFs is both a blessing and a curse. With many thousands of MOFs yet to be tested, it is highly likely that MOFs having superior properties for CO_2 capture exist. However, experimental testing of all candidates is impractical. Consequently, there is growing interest in the use of computational screening to identify promising CO_2 adsorbents.[22,28,29] Such an approach would reduce the number of compounds that must be synthesized and tested, thereby accelerating the discovery of optimal materials.

As a screening parameter, the energetics (i.e., enthalpy) of CO_2 adsorption is of particular importance as it impacts the capacity, selectivity, and efficiency of the carbon capture process. While it is possible to accurately predict thermodynamics using quantum chemical (QC) methods,[30] these methods are computationally expensive and are applicable only to cluster models that neglect the crystalline morphology of MOFs and possibly introduce finite-size effects; therefore, screening based on QC calculations would be inefficient. On the other hand, density functional theory calculations are capable of addressing the large unit cells typical of MOFs without resorting to cluster models. Unfortunately, conventional density functionals yield rather poor predictions of CO_2 adsorption thermodynamics,[31] as they do not account for long-range van der Waals (vdW) interactions. These interactions are believed to have a significant impact on the energetics and structure of these systems; thus the absence of vdW interactions has limited the applicability of DFT in modeling CO_2 uptake in MOFs. For example, using a conventional GGA functional, Wu et al.[31] reported an enthalpy of adsorption of 20 kJ/mol for CO_2 adsorption in Mg/DOBDC, which significantly underpredicts the experimental value of 47 kJ/mol.[20]

The inclusion of vdW interactions in density functional theory (DFT)[32] is an active area of research, and several approaches[33−41] have been proposed. Two notable methods are the semiempirical approach of Grimme, variously referred to as DFT-D1,[42] DFT-D2,[43] and DFT-D3,[44] and the nonempirical vdW-DF method of Dion et al.[45] These methods have demonstrated improved accuracy at moderate computational cost across a range of chemical environments.[34,46−51]

The DFT-D methods[42−44] involve the addition of a damped dispersion term (E_{disp}) to the Kohn−Sham DFT energy (E_{KS-DFT}). A similar scheme has been proposed by Wu et al.[52] The accuracy of all of the DFT-D methods[42−44] depends on the atomic dispersion coefficient, C_6 (e.g., see eq 2 in the methods section). In the DFT-D1 method,[42] this term is derived from experimental molecular polarizability data,[53] which, unfortunately, can be scarce for heavier elements. In the subsequent DFT-D2 implementation,[43] the C_6 coefficients are derived from computed atomic ionization potentials and polarizabilities. Elements in the same row of a given transition metal series are treated as having identical dispersion parameters,[43] taken as the average of the preceding group VIII and following group III elements. DFT-D2 has been shown to yield accurate experimental binding energies and equilibrium bond lengths for dimers of Krypton;[54] it improves the interlayer binding energy, layer−layer spacing, lattice parameters, and bulk moduli in layered solids such as graphite;[46,49,55,56] it also provides better agreement with quantum chemical reference data for the binding energies of weekly interacting dimers[43,57] in the S22 training set.[58] Regarding CO_2 adsorption, Valenzano and co-workers have shown that this approach can partially correct for the underbinding observed in B3LYP calculations for CO_2 on Mg/DOBDC.[30]

In contrast to the empirical underpinnings of the DFT-D2 approach, the vdW-DF method[45] includes vdW interactions in a nonempirical fashion. Initial tests of the vdW- DF method demonstrated improved accuracy in describing interactions in noble gas and benzene dimers.[45,59] Several other systems have since been explored with this formalism, including water interactions with benzene and other polycyclic aromatic hydrocarbons;[60,51] biomolecules such as nucleobase pairs and DNA, in which H-bonding and stacking interactions are crucial;[61,62] layered solids such as graphite and V_2O_5;[55,63] and physisorption of molecules onto surfaces[34,64] and within porous materials.[65] In these systems, the vdW-DF method showed improved agreement with experimental data or QC predictions, and generally outperformed conventional density functional calculations.

More recently, Klimes et al.[66,67] have demonstrated that the performance of the vdW-DF can depend sensitively upon the choice of the exchange functional. For example, by replacing the revPBE-based functional employed in ref 45 with a modified B88 functional[66] (referred to as the "optB88" functional), more accurate binding energies were obtained for the methane dimer and for the S22[58] test set. Mean absolute deviations from reference CCSD(T) binding data for this set decreased from ∼6 kJ/mol using revPBE-vdW to ∼1 kJ/mol for optB88-vdW. Klimes et al.[66,67] also explored three other exchange functionals: "optPBE", "optB86b", and "rPW86."[68] However, benchmarking on the S22 set revealed that the accuracy of these functionals was less than for optB88.

Given the large improvements reported in refs 66 and 67, upon altering the exchange functional, the goal of this study is to benchmark these same vdW functionals, along with the DFT-D2 method and conventional LDA and PBE-GGA functionals, against experimental enthalpies for CO_2 adsorption across four MOFs: M/DOBDC (M = Mg, Ni, Co) and HKUST-1.[69−73] All of the selected MOFs contain coordinatively unsaturated metal sites (CUS). These compounds are of interest because the presence of CUS correlates with high CO_2 uptake at low pressures,[19] presumably due to stronger CO_2−metal interactions. In addition, the thermodynamics of CO_2 adsorption in these systems have been experimentally measured by multiple groups,[20,74−82] adding to the reliability of the data.

Our calculations demonstrate that the LDA and PBE-GGA partially capture trends in the experimental ΔH values; nevertheless, these functionals significantly overbind (LDA) and underbind (GGA) CO_2 with respect to the experimental data. The addition of a semiempirical C_6R^{-6} dispersion term to the GGA exchange-correlation energy using "off the shelf" DFT-D2 parameters results in a substantial improvement in both the magnitude of the adsorption enthalpies and the trends across compounds. However, on average this approach still underbinds CO_2 as compared to the experimental data by 7 kJ/mol CO_2 (∼18% of the experimental ΔH). Improved accuracy can be obtained with some of the vdW density functionals. In

dx.doi.org/10.1021/jp3051164 | J. Phys. Chem. C 2012, 116, 16957−16968

particular, the revPBE functional yields a low absolute average error of only 2 kJ/mol CO_2 (4%) relative to experiment. This improvement in energetics is accompanied by a slight decrease in the accuracy of geometries, as the revPBE functional overestimates the metal−CO_2 bond length by about 10%. Our results are in good agreement with a nearly simultaneous study of CO_2 adsorption in Mg/DOBDC, which compared several vdW density functionals.[83] The identification of an efficient vdW density functional capable of accurately predicting the thermodynamics of CO_2 adsorption will facilitate computational screening for optimal carbon capture materials.

COMPUTATIONAL BACKGROUND

DFT-D2 Method. The DFT-D2[43] method, similar to its successor DFT-D1,[42] adds a dispersion contribution, E_{disp}, to the conventional Kohn−Sham DFT energy, E_{KS-DFT}, to give a dispersion-corrected total energy:

$$E_{DFT\text{-}D2} = E_{KS\text{-}DFT} + E_{disp} \quad (1)$$

The form of E_{disp} is given by:

$$E_{disp} = s_6 \sum_{i<j} \frac{C_6^{ij}}{R_{ij}^6} f_{dmp}(R_{ij}) \quad (2)$$

where $f_{dmp}(R_{ij}) = 1/(1 + e^{-d(R_{ij}/R_0^{ij}-1)})$, $C_6^{ij} = (C_6^i C_6^j)^{1/2}$, and $R_0^{ij} = R_0^i + R_0^j$. Here, C_6^i is the atomic dispersion coefficient, which is determined from DFT-PBE0[84] calculations of atomic ionization potentials (I_p) and static dipole polarizabilities (α) through the empirical relation $C_6 = 0.05NI_p\alpha$. N assumes values of 2, 10, 18, 36, and 54 for atoms from rows 1−5 of the periodic table. The factors 0.05 and N are chosen to reproduce the experimental binding energies and bond distances of rare gas dimers (Ne−Xe) and some weakly interacting complexes.[43] s_6 is a global scaling factor, which depends upon the specific density functional employed, R_0^i is the van der Waals radius of the ith atom (computed as before[42] but with a scaling factor 1.10), d determines the steepness of the damping function, and R_{ij} is the interatomic distance between atoms i and j. f_{dmp} is a damping function used to avoid singularities at small R_{ij} and to minimize dispersion contributions from interactions within typical (i.e., covalent) bonding distances. Our DFT-D2 calculations employ the PBE-GGA[85] functional and therefore follow the convention of using s_6 = 0.75 and a damping parameter d = 20.[43] The atomic dispersion coefficient and van der Waals radii are set to default values, which are summarized in the Supporting Information (Table 4). The maximum range of the dispersion interaction E_{disp} is set to 30 Å.

vdW-DF Method. The vdW-DF methods take as their starting point the adiabatic-connection fluctuation−dissipation (ACFD) theorem[86] and plasmon-pole approximation for the response of electron density. In this method,[45] the correlation energy is divided into local and nonlocal parts, $E_c = E_c^0 + E_c^{nl}$, with the total exchange-correlation energy given by:

$$E_{xc} = E_x^{GGA} + E_c^0 + E_c^{nl} \quad (3)$$

Here, E_x^{GGA} is GGA exchange energy, and the local part of the correlation energy, E_c^0, is treated with the LDA. (The sum of the first two terms in eq 3, plus the GGA correlation energy, E_c^{GGA}, give rise to the standard DFT-GGA exchange-correlation energy, $E_{KS\text{-}DFT}$.) The nonlocal component, E_c^{nl}, accounts for long-ranged electron correlation effects responsible for van der Waals interactions and is evaluated using a double integral over electron densities (r) at two different locations, r and r':

$$E_c^{nl} = \frac{1}{2}\int\int \rho(r)\Phi(r, r')\rho(r')\mathrm{d}r\,\mathrm{d}r' \quad (4)$$

Here, $\Phi(r, r')$ is a nonlocal kernel, which is a function of the charge density, its gradient at r and r', and $|r - r'|$. Evaluation of eq 4 can be expedited by tabulating $\Phi(r, r')$ in terms of r and r' in advance. Additional information can be found in ref 45.

As mentioned in the Introduction, in this study we consider the following vdW-DFs: revPBE-vdW, which is the "original" vdW-DF introduced in ref 45, and the four variants introduced by Klimes and co-workers,[66,67] optB86b, optB88, optPBE, and Lee et al.,[68] rPW86. The latter four functionals differ from the revPBE-vdW in their choice of the exchange energy, E_x^{GGA}, corresponding to the first term on the right-hand side of eq 3.

COMPUTATIONAL DETAILS

First principles DFT calculations were performed using the VASP code.[87] The projector-augmented-wave (PAW) method[88] was used to describe interactions between core and valence electrons. Spin polarized calculations were performed for those MOFs containing transition metals (i.e., Co, Ni, Cu). The plane-wave cutoff energy was set to 500 eV.

As previously mentioned, our calculations are aimed at evaluating the heat of adsorption (ΔH) of CO_2 in four MOFs containing coordinatively unsaturated metal sites (CUS). Three of the MOFs are isostructural variants of M/DOBDC,[20,69−72] where M = Ni, Mg, Co, with the fourth being Cu-HKUST-1.[73] The atomic structures of Ni/DOBDC and HKUST-1 were obtained from published literature data;[69,73] initial structures for Mg and Co/DOBDC were created by substituting Mg and Co for Ni in Ni/DOBDC. The primitive unit cells of DOBDC and HKUST-1 contain 54 and 156 atoms with 6 and 12 open metal sites, respectively. MOF structures containing adsorbed CO_2 were constructed from diffraction measurements[31,79] on Ni/DOBDC and HKUST-1. These measurements exhibit one CO_2 adsorption site per CUS metal.[31,79] Similar to what was done for the bare MOF structures, metal substitution was used to generate initial geometries for Mg and Co/DOBDC containing adsorbed CO_2. Including adsorbed CO_2 molecules, the primitive cells used in our calculations contained 72 atoms in the case of M/DOBDC-based systems, and 192 atoms for HKUST-1-based systems. All calculations on DOBDC-based compounds employed space group $R\bar{3}$ (No. 148); for HKUST-1, groups $Fm\bar{3}$ (No. 202) and $Fm3\bar{m}$ (No. 225) were used, respectively, for supercells with and without CO_2.

The energy of adsorption per CO_2 molecule was calculated using eight different forms for the energy functional. These include the Ceperley-Alder LDA,[89] PBE GGA,[90] Grimme's DFT-D2 method,[43] and five vdW-DFs in which the exchange-correlation energy is given by one of optB86b-vdW,[67] optB88-vdW,[66] optPBE-vdW,[66] revPBE-vdW,[45] and the modified PW86 functional, referred to as rPW86-vdW.[68,91] Adsorption energies ΔE were calculated using the following expression:

$$\Delta E = \frac{1}{n}(E_{MOF+CO_2} - E_{MOF} - nE_{CO_2}) \quad (5)$$

where, E_x is, respectively, the total energy of the CO_2-containing MOF, the MOF itself, and a CO_2 molecule. The number of adsorbed CO_2 molecules contained in the MOF unit cell is given by n. The energy of an isolated CO_2 molecule was evaluated using a supercell of dimension 10 × 11 × 12 Å. The

dx.doi.org/10.1021/jp3051164 | J. Phys. Chem. C 2012, 116, 16957−16968

Table 1. Comparison of Calculated CO_2 Adsorption Energies (in kJ/mol CO_2) with Experimental Data[a]

system	method	ΔE	ΔE_{vdW}	ΔE_{ZPE}	ΔE_{TE}	ΔH	% error	ΔH from experiments
Mg/DOBDC	LDA	−52.3		2.4	−1.3	−51.2	15.8	**−44.2** ± 4.6 (47,[20] 47,[74] 39,[75]43,[76] 39,[76] 42.8,[77] 51.6[78])
	PBE	−22.0		1.9	−0.1	−20.2	−54.3	
	DFT-D2	−43.4	−21.4	2.2	1.5	−39.7	−10.2	
	optB86b-vdW	−56.2	−34.2	2.1	0.2	−53.9	21.9	
	optB88-vdW	−55.5	−33.5	2.6	0.1	−52.8	19.5	
	optPBE-vdW	−58.7	−36.7	2.1	−0.6	−57.2	29.4	
	revPBE-vdW	−50.9	−28.9	2.1	1.5	−47.3	7.0	
	rPW86-vdW	−48.2	−26.2	2.1	−0.1	−46.2	4.5	
	revPBE-vdW[c]	−51.5						
	B3LYP+D*[30]	−41.5	−23.3	2.1	1.6	−37.9	−14.3	
	MP2:B3LYP+D*[30]	−46.3				−42.7	−3.4	
	LDA[31]	−51.2						
	PBE[31]	−20.2						
Ni/DOBDC	LDA							**−39.6** ± 1.5 (41,[20] 38,[76] 38,[76] 41.1,[78] 40[79])
	PBE	−12.0		1.8	1.4	−8.8	−77.8	
	DFT-D2	−34.8	−22.8	2.9	1.3	−30.6	−22.7	
	optB86b-vdW	−48.6	−36.6	2.4	0.6	−45.6	15.2	
	optB88-vdW	−47.9	−35.9	3.0	1.8	−43.1	8.8	
	optPBE-vdW	−49.8	−37.8	2.5	0.7	−46.6	17.7	
	revPBE-vdW	−41.3	−29.3	1.7	1.8	−37.8	−4.5	
	rPW86-vdW	−39.1	−27.1	3.1	1.5	−34.5	−12.9	
	revPBE-vdW[c]	−42.6						
	B3LYP+D*[30]	−38.9	−26.9	2.0	1.4	−35.5		
	MP2:B3LYP+D*[30]	−43.9				−40.5		
Co/DOBDC	LDA	−39.4		2.0	0.8	−36.6	2.5	**−35.7** ± 1.9 (37,[20] 34.3[78])
	PBE	−9.6		1.4	−0.1	−8.3	−76.8	
	DFT-D2	−31.1	−21.5	1.7	0.4	−29.0	−18.8	
	optB86b-vdW	−43.9	−34.3	1.7	1.8	−40.4	13.2	
	optB88-vdW	−43.6	−34.0	2.0	1.7	−39.9	11.8	
	optPBE-vdW	−46.0	−36.4	1.6	0.7	−43.7	22.4	
	revPBE-vdW	−39.3	−29.7	1.6	0.5	−37.2	4.2	
	rPW86-vdW	−36.2	−26.6	1.8	1.9	−32.5	−9.0	
	revPBE-vdW[c]	−40.0						
Cu-HKUST-1	LDA	−31.5		1.7	−0.8	−30.6	29.1	**−23.7** ± 8.2 (35,[80] 25,[80] 30,[81] 27.5,[78] 21.5,[78] 12.1,[82] 14.6[82])
	PBE	−8.9		2.7	−3.2	−9.4	−60.3	
	DFT-D2	−22.5	−13.6	4.8[b]	−0.8[b]	−18.5	−21.9	
	optB86b-vdW	−29.4	−20.5	4.8[b]	−0.8[b]	−25.4	7.2	
	optPBE-vdW	−31.7	−22.8	4.8[b]	−0.8[b]	−27.7	16.9	
	revPBE-vdW	−27.3	−18.4	4.8[b]	−0.8[b]	−23.3	−1.7	
	rPW86-vdW	−25.5	−16.6	4.8[b]	−0.8[b]	−21.5	−9.3	
	revPBE-vdW[c]	−27.1						
	DFT/CC[104]	−31.5						
	LDA[31]	−32.7						
	PBE[31]	−7.3						

[a] ΔE refers to the static 0 K adsorption energy, which omits zero point energies (ΔE_{ZPE}), and thermal contributions to the enthalpy (ΔE_{TE}). ΔH is the adsorption enthalpy at T = 300 K. ΔE_{vdW} is defined as the difference in static 0 K adsorption energies between dispersion-corrected and conventional PBE-GGA-based density functional methods. Adsorption enthalpies measured by several experiments at low CO_2 coverages, and their average and standard deviation, are summarized in the last column. "% Error" refers to the error of the calculated ΔH value with respect to the average experimental ΔH. Data for Ni/DOBDC within the LDA and for Cu-HKUST-1 within optB88-vdW are not reported due to difficulties associated with converging to the ground-state magnetic configuration. [b] ZPE and TE contributions for the vdW density functionals were evaluated using DFT-D2. [c] In this calculation, revPBE-vdW was used to relax cell parameters and ionic positions. In all other calculations, the lattice constants adopt the PBE-GGA values.

bond length of free CO_2 was calculated to be 1.168 Å in the LDA, and ranged from 1.174 to 1.179 Å in the GGA and the GGA-based DFT-D2 or DF-vdW methods. In comparison, the experimental bond length is 1.161 Å.[92]

k-point convergence testing was performed on the Mg/DOBDC and HKUST-1 supercells using mesh densities of 1 × 1 × 1, 2 × 2 × 2, and 3 × 3 × 3. The variation of CO_2 binding energies (ΔE) at 0 K with respect to *k*-point sampling density is shown in the Supporting Information (Table 5). We find that a *k*-point mesh of 1 × 1 × 1 is sufficient to converge CO_2 binding energies to within 0.3 and <0.1 kJ/mol, respectively, for Mg/DOBDC and HKUST-1. Hence, all calculations employ a 1 × 1 × 1 (Γ-point only) mesh.

The structures of the four empty MOFs and their respective CO_2-containing variants were initially optimized by relaxing the unit cell lattice parameters and atomic positions using the LDA

dx.doi.org/10.1021/jp3051164 | J. Phys. Chem. C 2012, 116, 16957−16968

Table 2. Heats of CO_2 Adsorption as a Function of Temperature, Pressure, and Loading As Measured by Various Experiments in the Literature[a]

				loading			
system	ΔH (kJ/mol)	temperature (K)	pressure (kPa)	wt %	(mol CO_2)/(kg MOF)	(no. CO_2)/metal site	method for ΔH calculation
Mg/DOBDC	−47	273, 296	∼0	0.50	0.11	0.01	Toth, Clausius−Clapeyron[20]
	−47	232−303	NR	NR			Langmuir, van't Hoff[74]
	−43	278−298	1−4	18.13	4.12	0.50	from isotherm[76]
	−39	278−298	3−8	24.30	5.52	0.67	from isotherm[76]
	−42.8	278−318	0−107	NR			Sip model[77]
	−73	278−318	∼0	0.88	0.20	0.02	Langmuir, Clausius−Clapeyron[77]
	−51.6	311	10	21.70	4.93	0.60	Toth, van't Hoff[78]
	−39	273−298	NR	NR			virial-type expansion[75]
Ni/DOBDC	−41	273, 296	∼0	0.50	0.11	0.02	Toth, Clausius−Clapeyron[20]
	−38	278−298	2−7	14.13	3.21	0.50	from isotherm[76]
	−38	278−298	4−9	18.93	4.30	0.67	from isotherm[76]
	−41.1	311	10	13.11	2.98	0.46	Toth, van't Hoff[78]
	−40	303−353	∼8	7.00	1.59	0.25	TSA (isosteric method)[79]
Co/DOBDC	−37	273, 296	∼0	0.50	0.11	0.02	Toth, Clausius−Clapeyron[20]
	−34.3	311	10	7.92	1.80	0.28	Toth, van't Hoff[78]
Cu-HKUST-1	−35	120−290	NR	0.44	0.10	0.02	SIM[80]
	−25	120−290	NR	23.77	5.40	1.09	SIM[80]
	−30	298−378	NR	NR			PSA (DTA)[81]
	−27.5	311	10	1.76	0.40	0.08	Toth, van't Hoff[78]
	−21.5	311	10	1.85	0.42	0.08	Toth, van't Hoff[78]
	−12.1	300	0.2−133	NR			Langmuir[82]
	−14.6	300	∼0	NR			TAP[82]

[a] CO_2 loading is expressed in three forms: weight percent (wt %)(g CO_2)/(g MOF) × 100; (mol CO_2)/(kg MOF); and number of CO_2 molecules per metal site within the MOF. NR, not reported; PSA, pressure swing adsorption; TSA, temperature swing adsorption; SIM, sorption isosteric method; DTA, differential thermal analysis; TAP, temporal analysis of products.

or PBE-GGA. To assess the impact of van der Waals contributions on geometries, structure optimizations were also performed using the revPBE-vdW. The optimized lattice parameters for these MOFs and their corresponding MOF +CO_2 systems are given in the Supporting Information (Table 6), and are compared to experimental data. In general, the agreement between the predicted and measured lattice constants is very good. Consistent with prior reports, the average LDA lattice constants are slightly smaller than the experimental values, while the PBE-GGA and revPBE-vdW predictions are slightly larger. As the difference between the PBE-GGA and revPBE-vdW lattice constants is small, 1−2%, structural differences between functionals result in negligible changes to adsorption energies on the order of 1 kJ/mol CO_2. (See Table 1 for a comparison of revPBE-vdW adsorption energies calculated with the PBE-GGA and revPBE-vdW lattice constants.) Consequently, the relaxed PBE-GGA lattice constants were used in subsequent adsorption energy calculations employing the DFT-D2 and vdW-DF methods. In the latter cases, the atomic coordinates were reoptimized by minimizing atomic forces to a tolerance of less than 0.01 eV Å. Regarding the impact of CO_2 adsorption on MOF volume, neutron diffraction experiments by Queen et al.[93] found that the volume of Mg/DOBDC varied by less than 0.4% upon adsorption of 1 CO_2 per Mg site. Similarly, computed cell volumes for all functionals change by a negligible amount upon CO_2 adsorption, Supporting Information Table 6.

The ground-state magnetic configuration and corresponding magnetic moments were determined for the relaxed MOFs with and without adsorbed CO_2. The presence of adsorbed CO_2 was found to have a negligible effect on magnetic properties. In the case of Co and Ni/DOBDC, a ferromagnetic ground state was observed with respective magnetic moments of ∼3 and ∼2 μ_B per metal atom. On the other hand, Cu spins in HKUST-1 adopt an antiferromagnetic configuration with a moment of 0.55 μ_B.

The initial binding energies (ΔE) obtained by our calculations are static, 0 K energies and do not include zero point (E_{ZPE}) and thermal energy (E_{TE}, T = 0 → 300 K) contributions. To compare with experimental measurements of CO_2 adsorption enthalpies at room temperature, finite-temperature enthalpic contributions were calculated within the harmonic approximation.[94,95] Normal-mode vibrational frequencies were determined for the relaxed DFT-D2 and vdW-DF structures using the so-called direct method.[96] For supercells containing MOFs or MOFs with adsorbed CO_2, thermal energy contributions arise only from vibrational contributions. Thus, the enthalpy of a MOF or MOF+CO_2 supercell can be written as:

$$H^{MOF} = E0 + E_{ZPE} + E_{TE} \quad (6)$$

where $E0$ is the static total energy, $E_{ZPE} = \sum_i \hbar\omega_i/2$, E_{TE} is the thermal energy due to vibrational contributions, $E_{TE} = \sum_i \hbar\omega_i/[\exp(\hbar\omega_i/k_BT) - 1]$, k_B is the Boltzmann constant, and ω_i is the vibrational frequency for the ith normal mode. In contrast, the enthalpy of gas-phase CO_2 is given by an identical expression plus an additional contribution of 7/2 k_BT arising from translational, rotational, and PV degrees of freedom. Replacing E by E_{ZPE} and E_{TE} on the right-hand side of eq 5 allows for the isolation of ZPE (ΔE_{ZPE}) and thermal energy contributions (ΔE_{TE}) to the adsorption energy. Taking into account the ZPE and TE, the adsorption enthalpy is calculated as $\Delta H = \Delta E + \Delta E_{ZPE} + \Delta E_{TE}$. We set T = 300 K in all of our calculations. Finally, we define the static dispersion energy

dx.doi.org/10.1021/jp3051164 | J. Phys. Chem. C 2012, 116, 16957−16968

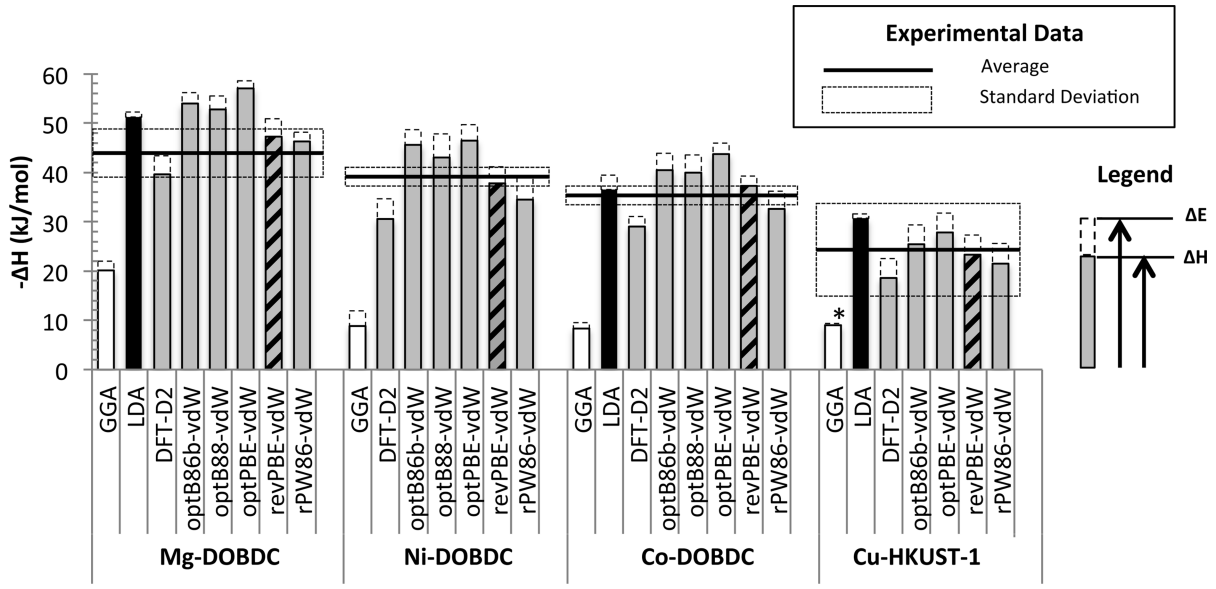

Figure 1. CO_2 adsorption energies in M/DOBDC (M = Mg, Ni, Co) and HKUST-1 calculated using standard density functional methods (LDA and GGA), the semiempirical DFT-D2 method of Grimme, and five nonempirical GGA-based vdW density functionals. The black, white, and gray columns depict adsorption enthalpies (ΔH) calculated with LDA, PBE-GGA, and vdW DFT methods, respectively. (Gray/black cross-hatching is used to highlight the revPBE-vdW functional, which yields the best agreement with experimental data.) The total column height represents the 0 K static binding energy, and the dashed segment at the top indicates the sum of zero point (ZPE) and thermal energy (TE) contributions at T = 300 K. The average experimental ΔH is given as a horizontal line; the standard deviation in the experimental data is given by a dashed box. * ZPE+TE contribution for Cu-HKUST-1 in the PBE-GGA sum to −0.5 kJ/mol.

contribution arising from use of vdW-corrected density functionals as ΔE_{vdW}. This contribution is calculated relative to the static PBE-GGA binding energy such that $\Delta E_{vdW} = \Delta E_{vdW\text{-}DFT} - \Delta E_{PBE}$.

RESULTS AND DISCUSSION

Adsorption Energies. Calculated CO_2 adsorption energies (ΔE) and enthalpies (ΔH) in M/DOBDC (M = Mg, Ni, Co) and Cu-HKUST-1 across all eight examined functionals are reported in Table 1. We adopt a sign convention in which negative energies/enthalpies correspond to an exothermic adsorption interaction. The calculated values are compared to adsorption data from 21 experimental measurements culled from the recent literature.[20,74−76,78,80−82] The MOFs examined in this study were chosen on the basis of the existence of at least two independent and consistent experimental measurements of the CO_2 adsorption enthalpy. Because our calculations model the low coverage regime of one CO_2 per metal site, we have selected experimental data at low CO_2 partial pressures, typically less than 10 kPa. A comprehensive listing of the details for each experiment, including temperature, pressure, loading, and methods used, is given in Table 2. Experimental data (e.g., −73 kJ/mol for Mg/DOBDC)[77] that differed significantly from the majority of other measurements were excluded. However, even with the exclusion of out-lying data, in cases such as HKUST-1 there remains a large spread in the experimental data. For this MOF, we identified seven enthalpy measurements, ranging from 12.1 to 35 kJ/mol. Presumably, the variation can be attributed to differences in sample handling, postsynthesis activation processes (i.e., cleanness of the MOF),[20,77] and numerical uncertainties associated with the isotherm fitting technique used to extract ΔH.[82,97,98] Because it is not obvious which data are most reliable, we compare the calculated enthalpies against the mean experimental ΔH for CO_2 adsorption in each MOF, which is given in bold type in Table 1. (The standard deviation of the experimental data is reported as "±" in Table 1 and with error bars in Figure 1.)

Conventional LDA and GGA Functionals. We first turn to results obtained using the conventional LDA and PBE-GGA functionals. As previously mentioned, these functionals do not account for long-ranged electron correlation effects such as vdW interactions. Consequently, we expect limited agreement with experimental data in environments where these interactions are important. This expectation is largely confirmed based on the static 0 K binding energy data (ΔE) in Table 1, which shows that the LDA and GGA systematically overbind (ca. 10−32%) and underbind CO_2 (<50%), respectively, in all four MOFs as compared to the experimental energies. Similar over- and underestimates between LDA and GGA have been reported for a range of other properties such as lattice parameters, bulk moduli, and atomization energies.[67,99−102] A distinction between the LDA and PBE-GGA is evident in their ability to reproduce the experimental trend in ΔH across the four MOFs: $\Delta H^{Mg/DOBDC} > \Delta H^{Ni/DOBDC} > \Delta H^{Co/DOBDC} > \Delta H^{Cu\text{-}HKUST\text{-}1}$. Whereas the LDA correctly captures this trend, the PBE-GGA is only partially successful in the regard as it predicts $\Delta H^{Cu\text{-}HKUST\text{-}1}$ to be more exothermic than $\Delta H^{Ni/DOBDC}$ and $\Delta H^{Co/DOBDC}$. Figure 1 provides a graphical depiction of the calculated adsorption energies and their comparison with experiments. Here, the height of the white and black bars represents the GGA and LDA ΔH values, respectively. The dashed portion at the top of each bar indicates the magnitude of zero point and thermal energy contributions. (In the case of Ni/DOBDC, we do not report energetics for the LDA functional due to difficulties in achieving convergence to the magnetic ground state.)

Our LDA and GGA binding energies are in good agreement with previous DFT calculations by Wu et al.[31] on Mg/DOBDC and Cu-HKUST-1. In the case of Mg/DOBDC, we find LDA

dx.doi.org/10.1021/jp3051164 | J. Phys. Chem. C 2012, 116, 16957−16968

(GGA) values of 52.3 (22.0) kJ/mol, while for Cu-HKUST-1 we find 31.5 (8.9) kJ/mol (see Table 1). Similarly, Wu et al. found LDA (PBE-GGA) values of 51.2 (20.2) kJ/mol for Mg/DOBDC, and 32.7 (7.3) kJ/mol for Cu-HKUST-1.

Because zero point and thermal energy contributions generally result in a more endothermic CO_2−MOF interaction (see Table 1), their inclusion in the underbound GGA data worsens agreement with experiment. On the other hand, these contributions have the opposite effect on the (overbound) LDA energies, improving agreement with experimental enthalpies to within approximately 15%. As we describe below, additional improvements are possible with functionals that account for vdW interactions.

Semiempirical DFT-D2 Method. We next examine the performance of the semiempirical DFT-D2 functional,[42,43] which was used in conjunction with the PBE-GGA. Our calculated dispersion-corrected adsorption energies (ΔE) and enthalpies (ΔH) are summarized in Table 1. In Figure 1 binding energies at 0 K are represented by the combined height of the gray columns and the dashed caps at top. In all of the MOFs examined, the dispersion contribution (ΔE_{vdW}) is significant, ranging from −13.6 kJ/mol in HKUST-1 to −22.8 kJ/mol in Ni/DOBDC. (The value of E_{disp} is roughly constant at −22 kJ/mol across the entire M/DOBDC series.) As a consequence of the large size of E_{disp}, the use of DFT-D2 results in a significant improvement in CO_2 adsorption enthalpies as compared to the underbound PBE-GGA. For example, in Mg/DOBDC, ΔH decreases from −20.2 kJ/mol (GGA) to −39.7 kJ/mol (DFT-D2), substantially improving agreement with the experimental value of −44.2 kJ/mol. This is similar to the value of −37.9 kJ/mol obtained with the B3LYP +D* functional.[30,74]

Factoring in zero point and thermal energy contributions, on average the DFT-D2 adsorption enthalpies are about 18% too endothermic as compared to the average experimental enthalpies. Nevertheless, the experimental trends in ΔH across the MOFs are correctly reproduced by this method. Given that the LDA already overbinds CO_2 in these MOFs, and that most efforts aimed at including vdW interactions into DFT focus on GGA-based functionals, we did not conduct LDA-based DFT-D2 calculations. (Presumably such an approach would worsen the overbinding behavior observed with the LDA alone.) We emphasize that the present results were obtained using "off the shelf" coefficients for the dispersion energy. We expect that additional improvements in accuracy could be obtained by optimization of the atomic dispersion coefficients. However, given the promising results obtained with the vdW-DF's (described below), such an optimization was not attempted.

van der Waals Density Functionals. Table 1 and Figure 1 also report the energetics of CO_2 adsorption predicted by the five vdW density functionals: optB86b-vdW, optB88-vdW, optPBE-vdW, rPW86-vdW (also known as vdW-DF2),[66,67,91] and the original revPBE-vdW.[45] As compared to DFT-D2, all of the vdW-DF's yield more exothermic vdW contributions, with values ranging from −16.6 to −22.8 kJ/mol in HKUST-1 and from −26.2 to −37.8 kJ/mol across the M/DOBDC series. While a more exothermic interaction would offset the underbinding observed in DFT-D2, in three of the five vdw-DF's the vdW contribution is so large that it results in overbinding of CO_2 with respect to experimental measurements. This is the case for optB86b-vdW, optB88-vdW, and optPBE-vdW, where inclusion of vibrational and thermal contributions yields ΔH values that are, respectively, 21.9%, 19.5%, and 29.4% more exothermic than the average experimental values for Mg/DOBDC. (In the case of HKUST-1, we do not report energetics for the optB88-vdW functional due to difficulties in achieving convergence to the antiferromagnetic spin state.[103])

In contrast to the overbinding observed for optB86b-vdW, optB88-vdW, and optPBE-vdW, the ΔH values predicted by revPBE-vdW and rPW86-vdW do not show a tendency for systematic under- or overprediction of CO_2 enthalpies. In general, these two functionals yield the best agreement with the experimental enthalpies. As shown in Table 1, the average error in ΔH with respect to the experimental data across all four MOFs is 8.9% for rPW86-vdW, and only 4.4% (∼2 kJ/mol) for revPBE-vdW. To place these values in context, we note that the standard deviation in the experimental ΔH values for the M/DOBDC series is 6.8%. For HKUST-1, the experimental uncertainty is much larger, 34.6%. Therefore, for the MOFs examined here, the revPBE-vdW method is capable of predicting adsorption thermodynamics with an accuracy comparable to that of experimental measurements.

Regarding trends in the binding energies, we note that the energies predicted by the vdW functionals across the different MOFs can be rank-ordered as: optPBE > optB86b > optB88 > revPBE > rPW86. That is, optPBE generally results in overbinding of CO_2, whereas rPW86 results in the weakest binding. As previously mentioned, for the vdW functionals considered here, the local and nonlocal correlation components of the exchange-correlation energy ($E_c^0 + E_c^{nl}$) are identical. Therefore, trends in the binding energies can be rationalized in terms of short-ranged repulsion arising from the differing functionals used for the exchange energy E_x^{GGA}.[66,67,83] More specifically, it has been shown that functionals having large values of the exchange energy enhancement factor $F_x(s)$ yield weaker binding, and vice versa. (F_x appears in the expression for the exchange energy density: $\epsilon_x(n,s) = \epsilon_x^{LDA}(n)F_x(s)$, where ϵ_x^{LDA} is the LDA exchange energy density and n is the charge density.)

Figure 4 in the Supporting Information plots F_x as a function of the reduced density gradient s. For Mg/DOBDC and Ca/BTT, it has been shown that the distribution of reduced density gradient values is peaked around $s = 1$. Assuming that the distribution is similar in the present systems, Figure 4 in the Supporting Information demonstrates that, with the exception of optPBE, the magnitude of F_x for the various functionals at $s = 1$ closely follows the trend in their relative binding energies. In the case of optPBE, the large overbinding can be explained by its preponderance of PBE exchange, which is known to result in attractive interactions in cases where it should not.[66]

Zero Point and Thermal Energy Contributions. In concluding this section, we comment on the significance of zero point energies (ΔE_{zpe}) and thermal energy contributions (ΔE_{TE}) to the adsorption enthalpy. As shown in 1, both ΔE_{zpe} and ΔE_{TE} are small in comparison to the vdW contributions. Within the M/DOBDC series, ΔE_{zpe} assumes a relatively constant value of approximately 2−3 kJ/mol; ΔE_{zpe} is slightly larger, ∼5 kJ/mol, in HKUST-1. As $\Delta E_{zpe} > 0$ in all cases, inclusion of ZPE contributions results in a more endothermic CO_2−MOF interaction. Calculated ΔE_{TE} contributions are on average smaller (∼1 kJ/mol) than those for ΔE_{zpe}, and in some cases (e.g., HKUST-1) are negative. (Because of the large unit cell of HKUST-1, phonon calculations were only attempted using the LDA, GGA, and DFT-D2 methods. ΔE_{zpe} and ΔE_{TE} values from the DFT-D2

dx.doi.org/10.1021/jp3051164 | J. Phys. Chem. C 2012, 116, 16957−16968

calculation were then used to estimate these contributions for the other vdW functionals.)

Inspection of the data in Table 1 and Figure 1 (dashed columns) indicates that in all but one of the cases studied (PBE-GGA for Cu-HKUST-1) the summed effect of ΔE_{zpe} and ΔE_{TE} is to shift MOF−CO_2 interactions to be more endothermic by about 2−4 kJ/mol. The small size and relative constancy of these contributions allow us to draw two conclusions: (1) Differences in accuracy between the different vdW functionals arise primarily from differences in static binding energies, ΔE, with vibrational contributions being less important. (2) In systems having large unit cells, one may approximate the room temperature enthalpy of adsorption ΔH by adding an endothermic shift of ∼3 kJ/mol to the static binding energy (ΔE) calculated using the revPBE-vdW method. Prior calculations using the DFT-D2 method in conjunction with the B3LYP functional found values of 2.1 and 1.6 kJ/mol for ΔE_{zpe} and ΔE_{TE}, respectively, in Mg/DOBDC.[30,74] Comparable values of 2.0 (ΔE_{zpe}) and 1.4 kJ/mol (ΔE_{TE}) were also reported for Ni/DOBDC.[30,74]

Structure. In addition to comparing adsorption thermodynamics across these systems, it is also instructive to characterize how their equilibrium geometries differ as a function of the energy functional employed. A typical optimized geometry for CO_2 adsorbed in Mg/DOBDC (obtained with the optB86b-vdW functional) is shown in Figure 2. Qualitatively similar geometries were obtained across all of the functionals examined in this study. For example, we find that CO_2 binds to the metal site in an end-on fashion through one O atom irrespective of the specific MOF examined or functional used. DFT studies by Wu et al.[31] and Valenzano et al.[74] also revealed similar binding geometries for CO_2 to the metal site in Mg/DOBDC and HKUST-1.

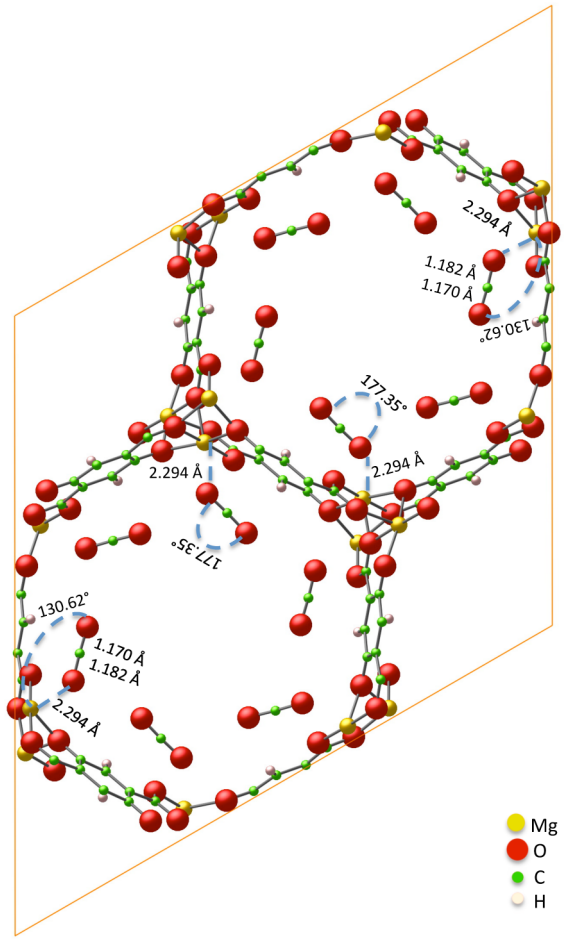

Figure 2. Optimized structure for CO_2 adsorbed on Mg/DOBDC as calculated using the optB86b-vdW functional.

Calculated bond lengths and bond angles are compared to experimental data for the Mg-, Ni-, and Cu-based MOFs from neutron[31,93] (for Mg/DOBDC and HKUST-1) and X-ray diffraction[79] (for Ni/DOBDC) experiments in Table 3. (To our knowledge, experimental structure data for Co/DOBDC have not been reported.) Tabulated properties include three bond lengths and two bond angles, where M···O refers to the bond length between the metal atom and closest oxygen in the adsorbed CO_2; C−O refers to the bond length between C and O in CO_2 involving the O farthest from the MOF metal site; MO−C is the distance between C and O in CO_2 involving the O closest to the metal site; ∠O−C−O is the angle formed by the O−C−O atoms within CO_2; and ∠M−O−C is the angle formed between the MOF metal site, its nearest-neighbor O (from CO_2), and the C atom within CO_2.

For the LDA and GGA functionals, the predicted metal−oxygen bond lengths M···O follow the trends observed for the static binding energies. That is, the overbound LDA adsorption energies ΔE_{LDA} result in shorter M···O bond lengths (∼ −4%) relative to the experimental data, while the underbound PBE energies yield M···O values that are too large (3−8%). This behavior is consistent with the notion that stronger CO_2−MOF interactions should result in shorter M···O distances. In contrast, for the six vdW-based functionals, there is no clear relationship between interaction strength and M···O distance. In fact, all of the vdW-based methods overpredict the experimental M···O bond length to varying degrees. Best agreement with the experimental data is achieved for the optB86b-vdW and optB88-vdW functionals (0.1−5% error), which generally overpredict the enthalpy of CO_2 adsorption. On the other extreme, revPBE-vdW and rPW86-vdW yield the largest errors in bond length (1.9−14.3%), despite having the best agreement with experimental enthalpies. Predicted M···O bond lengths for optPBE-vdW and DFT-D2 fall between these two groups (0.8−8%). In an earlier study, Valenzano et al.[74] calculated a M···O distance of 2.31 Å in Mg/DOBDC using the B3LYP+D* method. This is identical to our PBE-DFT-D2 value.

The effect of CO_2 loading upon the metal−oxygen length was examined for Mg/DOBDC using the revPBE-vdW, and a weak dependence was observed: M···O grows from 2.367 to 2.392 Å as the loading increases from 1/6 CO_2/Mg to 1 CO_2/Mg. On the other hand, experiments by Queen et al.[93] also found a small change in M···O (∼0.09 Å, for coverages between 0.24 and 0.89 CO_2/metal); however, in this case, M···O contracts rather expands.

Regarding bond angles, we find that across all eight functionals the computed metal−O−C angles ∠M−O−C are overestimated as compared to experimental data by ∼18° and ∼3°, respectively, in Mg/DOBDC and Ni/DOBDC, and underestimated by ∼6−7° in HKUST-1. An earlier study reported similar values in Mg/DOBDC.[74] The calculated deviation of adsorbed CO_2 from its linear geometry ∠O−C−O is relatively small, ∼2−4°, and is largely independent of the functional or choice of MOF. Our ∠O−C−O angles are similar to the DFT values reported by Wu et al.:[31] 175.0° (LDA) and

dx.doi.org/10.1021/jp3051164 | J. Phys. Chem. C 2012, 116, 16957−16968

Table 3. Comparison of Calculated Bond Lengths (Å) and Angles (deg) for CO_2-Containing MOFs with Experimental Data[a]

		M···O					
system	method	value	% error	MO−C	C−O	∠M−O−C	∠O−C−O
Mg/DOBDC	LDA	2.184	−4.73	1.175	1.162	129.20	176.12
	GGA	2.374	3.56	1.180	1.171	133.16	178.19
	DFT-D2	2.311	0.81	1.181	1.170	130.28	177.04
	optB86b-vdW	2.294	0.07	1.182	1.170	130.62	177.35
	optB88-vdW	2.288	−0.20	1.180	1.168	130.94	177.37
	optPBE-vdW	2.330	1.64	1.183	1.172	130.04	177.85
	revPBE-vdW	2.392	4.34	1.184	1.174	130.95	178.35
	rPW86-vdW	2.336	1.90	1.183	1.171	130.62	177.88
	experiment[31]	2.283 (0.64)		1.119	1.122	112.78	160.50
	experiment[93]	2.302 (0.89)		1.062	1.173	129.60	172.09
Ni/DOBDC	GGA	2.471	7.90	1.18	1.173	127.09	178.86
	DFT-D2	2.361	3.10	1.182	1.172	122.36	178.14
	optB86b-vdW	2.326	1.57	1.183	1.171	121.27	178.27
	optB88-vdW	2.340	2.18	1.181	1.170	121.53	178.26
	optPBE-vdW	2.426	5.94	1.183	1.173	120.84	178.66
	revPBE-vdW	2.617	14.28	1.183	1.176	120.29	179.02
	rPW86-vdW	2.470	7.86	1.183	1.173	121.29	178.61
	experiment[79]	2.29		1.21	1.21	117.00	162.00
Co/DOBDC	LDA	2.274		1.176	1.164	118.02	177.63
	GGA	2.665		1.179	1.174	126.09	179.12
	DFT-D2	2.594		1.181	1.173	116.78	178.29
	optB86b-vdW	2.513		1.182	1.173	118.06	178.43
	optB88-vdW	2.522		1.180	1.171	117.68	178.38
	optPBE-vdW	2.618		1.182	1.175	117.03	178.78
	revPBE-vdW	2.812		1.183	1.177	115.95	179.05
	rPW86-vdW	2.635		1.182	1.174	116.89	178.68
Cu-HKUST-1	LDA	2.330	−4.51	1.174	1.163	108.08	178.74
	GGA	2.633	7.91	1.181	1.172	108.37	179.02
	DFT-D2	2.637	8.07	1.181	1.172	108.30	179.03
	optB86b-vdW	2.562	5.00	1.181	1.172	108.44	179.15
	optPBE-vdW	2.635	7.99	1.182	1.173	108.78	180.00
	revPBE-vdW	2.771	13.57	1.184	1.176	106.55	180.00
	rPW86-vdW	2.684	10.00	1.182	1.173	107.83	179.22
	experiment[31]	2.440 (1.07)		1.322	1.396	114.45	158.04

[a]M···O refers to the bond length between the metal atom and closest oxygen atom in adsorbed CO_2; C−O refers to the bond length between C and O in CO_2 involving the oxygen farthest from the MOF metal site; MO−C is the distance between C and O in CO_2 involving the O atom closest to the metal site; ∠O−C−O is the angle formed by the atoms in a carbon dioxide molecule; and ∠M−O−C is the angle formed between the metal site, its neighboring oxygen in CO_2, and C in CO_2. The experimental data are at 20 K except for Ni, which is at 100 K. Where available, the experimental occupancy of CO_2 per metal site is given in parentheses.

178.0° (GGA) for Mg/DOBDC and 178.7° (LDA) and 179.0° (GGA) for HKUST-1. These computational predictions differ significantly from the experimental ∠O−C−O bond angle of approximately (∼160°). Wu et al.[31] suggested that the disagreement could arise from the thermal excitation of low energy CO_2 rotational modes about the metal with a span ±10°. Such rotations would increase uncertainties in the measurement of ∠O−C−O and ∠M−O−C.

We next turn to the C−O bond lengths within the adsorbed CO_2 molecule. In gas-phase CO_2, the C−O bond length is 1.161 Å.[92] Our calculations and experimental measurements find that in the adsorbed state these distances differ from those in free CO_2,[31,79] presumably due to interactions with the MOF metal site. In the case of experiments, the length of both C−O bonds varies inversely with ΔH, ranging from about 1.12 Å in Mg/DOBDC to more than 1.32 Å in HKUST-1. On the other hand, calculations predict these distances to be relatively independent of the MOF adsorbent, regardless of the functional used. With the exception of the Ni− DOBDC system, experiment and theory both predict the C−O bonds to be of unequal length. The calculated C−O bond lengths proximal to M are slightly elongated by ∼0.01 Å with respect to the distal one in all DFT calculations. Consistent with our findings, prior DFT[31] and B3LYP+D*[74] calculations also predicted a slight (0.01−0.02 Å) elongation of the C−O bond nearest the metal site. This result differs somewhat from the experimental measurements, which find a slight contraction of this bond length (relative to the C−O bond distal to M) in Mg/DOBDC and HKUST-1.

Regarding structural trends across the MOFs, our calculations predict a rough increase in bond length M···O and a gradual expansion in CO_2 bond angle ∠O−C−O starting from Mg/DOBDC and progressing to Ni and Co/DOBDC, and to Cu in HKUST-1. This trend follows the decreasing strength of interaction between the MOF and CO_2. Overall, we find that the optB86b-vdW functional yields the best agreement with the experimental geometries. On the other hand, the revPBE-vdW functional, which was the most successful at

dx.doi.org/10.1021/jp3051164 | J. Phys. Chem. C 2012, 116, 16957−16968

reproducing adsorption enthalpies, exhibits the largest errors in structural properties among the functionals benchmarked here.

CONCLUSION

Accurate computational methods are needed to predict the capacity, selectivity, and efficiency of porous materials for applications in gas capture and storage. Unfortunately, the most efficient and widely used method for calculating molecule–surface interactions, density functional theory, does not include long-range van der Waals interactions. These interactions are crucial for predicting thermodynamic properties in materials envisioned for carbon capture applications.

Toward the goal of identifying efficient computational schemes capable of predicting the performance of MOF-based adsorbents, in this study we have benchmarked six van der Waals density functionals (DFT-D2 and vdW-DF) with respect to experimental enthalpies for CO_2 adsorption in four prototype metal organic frameworks: M/DOBDC (M = Mg, Ni, Co) and Cu-HKUST-1. Prior studies have identified these systems as promising materials due to their unsaturated metal sites.

Regarding the conventional LDA and GGA functionals, we find that these methods only partially capture thermodynamic trends. Furthermore, they significantly overbind (LDA) and underbind (GGA) CO_2 with respect to the experimental enthalpies. The addition of a semiempirical r^{-6} dispersion term to the GGA exchange-correlation energy using "off the shelf" DFT-D2 parameters results in a substantial improvement in both the magnitude of the adsorption enthalpies and the ability to capture trends across systems. However, on average this approach still underbinds CO_2 as compared to the experimental data by ∼7 kJ/mol (18%). Better accuracy is obtained with some of the nonempirical vdW density functionals, with the revPBE-based functional of Dion et al. yielding an average error of only ∼2 kJ/mol (4%) relative to experiment. This improvement in energetics is accompanied by a slight decrease in the accuracy of predicted structures, as the revPBE overestimates the metal–CO_2 bond length by about 10%.

Regarding the generality of our results, we note that the present study is restricted to CO_2 adsorption in MOFs having coordinatively unsaturated metal sites. Nevertheless, the systems considered exhibit two different coordination geometries for the metal sites, and have ion identities spanning the alkaline earth metals (Mg), as well as transition metals having partial (Ni, Co) and full d shells (Cu). Consequently, our results appear to be independent of the choice of metal ion. Further study is needed to examine the performance of these functionals for adsorption of other molecules across the broader class of MOF compounds. In this regard, the availability of high-quality experimental data is also essential.

The efficiency and accuracy of the revPBE-vdW functional suggests that density functional methods are viable for rapid screening of potential CO_2 adsorbents. The ability of such an approach to address the large, periodic unit cells typical of MOFs offers advantages over expensive, cluster-based quantum-chemical methods.

ASSOCIATED CONTENT

Supporting Information

Equation of state fits to cell energy versus volume calculations, relaxed lattice constants and cell volume data, *k*-point convergence data, dispersion parameters used in the DFT-D2 calculations, and a plot of the exchange enhancement factor for the various vdW density functionals. This material is available free of charge via the Internet at http://pubs.acs.org.

AUTHOR INFORMATION

Corresponding Author

*E-mail: djsiege@umich.edu.

Notes

The authors declare no competing financial interest.

ACKNOWLEDGMENTS

We thankfully acknowledge Jiří Klimeš for providing the vdW-DF routines implemented in the VASP code. Computational resources and support were provided by the University of Michigan Center for Advanced Computing. J.H. is grateful for financial support from the UM Summer Undergraduate Research in Engineering (SURE) Program.

REFERENCES

(1) Core Writing Team. Pachauri, R. K., Reisinger, A., Eds. *Climate Change 2007: Synthesis Report; Intergovernmental Panel on Climate Change*; IPCC: Geneva, Switzerland, 2007.
(2) Energy Information Administration, E., Annual Energy Outlook 2006, 2006.
(3) Energy Information Administration, E., International Energy Outlook 2006, 2006.
(4) Energy Information Administration, E., Emissions of Greenhouse Gases in the United States 2005, 2006.
(5) *Carbon Dioxide Emissions from the Generation of Electric Power in the United States*; Environmental Protection Agency: Washington, DC, 2000.
(6) Figueroa, J. D.; Fout, T.; Plasynski, S.; McIlvried, H.; Srivastava, R. D. *Int. J. Greenhouse Gas Control* **2008**, *2*, 9–20.
(7) Aaron, D. T. C. *Sep. Sci. Technol.* **2005**, *40*, 321–348.
(8) Freeman, B. *Assessment of Post-Combustion Carbon Capture Technology Developments*; Electric Power Research Institute (EPRI): Technical Update 1012796, 2007.
(9) Kim, I.; Svendsen, H. F. *Ind. Eng. Chem. Res.* **2007**, *46*, 5803–5809.
(10) Yong, Z.; Mata, V.; Rodrigues, A. E. *Sep. Purif. Technol.* **2002**, *26*, 195–205.
(11) National Energy Technology Laboratory, N., Cost and Performance Baseline for Fossil Energy Plants, 2007.
(12) Yang, R. T. *Adsorbents: Fundamentals and Applications*; John Wiley & Sons, Inc.: New York, 2003.
(13) Choi, S. J.; Drese, H.; Jones, C. W. *ChemSusChem* **2009**, *2*, 796–854.
(14) Ferey, G. *Chem. Soc. Rev.* **2008**, *37*, 191–214.
(15) Rowsell, J. L. C.; Yaghi, O. M. *Microporous Mesoporous Mater.* **2004**, *73*, 3–14.
(16) Batten, S. R.; Neville, S. M.; Turner, D. R. *Coordination Polymers: Design, Synthesis, and Application*; Royal Society of Chemistry: Cambridge, UK, 2009.
(17) Hong, M.-C., Chen, L., Eds. *Design and Construction of Coordination Polymers*; John Wiley & Sons, Inc.: Hoboken, NJ, 2009.
(18) Long, J. R.; Yaghi, O. M. *Chem. Soc. Rev.* **2009**, *38*, 1213–1214.
(19) Keskin, S.; van Heest, T. M.; Sholl, D. S. *ChemSusChem* **2010**, *3*, 879–891.
(20) Caskey, S. R.; Wong-Foy, A. G.; Matzger, A. J. *J. Am. Chem. Soc.* **2008**, *130*, 10870–10871.
(21) Park, T.-H.; Cschosz, K. A.; Wong-Foy, A. G.; Dailly, A.; Matzger, A. J. *Chem. Commun.* **2011**, *47*, 1452–1454.
(22) Wilmer, C. E.; Leaf, M.; Lee, C. Y.; Farha, O. K.; Hauser, B. G.; Hupp, J. T.; Snurr, R. Q. *Nat. Chem.* **2012**, *4*, 83–89.
(23) Ockwig, N. W.; Delagodo-Friedrichs, O.; Okeeffe, M.; Yaghi, O. M. *Acc. Chem. Res.* **2005**, *38*, 176–182.
(24) Koh, K.; Wong-Foy, A. G.; Matzger, A. J. *J. Am. Chem. Soc.* **2009**, *131*, 4184–4185.

(25) Furukawa, H.; Ko, N.; Go, Y. B.; Aratani, N.; Choi, S. B.; Choi, E.; Yazaydin, A. O.; O'Keeffe, M.; Yaghi, O. M. *Science* **2010**, *329*, 424−428.
(26) Yuan, D.; Zhao, D.; Sun, D.; Zhou, H.-C. *Angew. Chem., Int. Ed.* **2010**, *49*, 5357−5361.
(27) Farha, O. K.; Yazzaydin, A. O.; Eryazici, I.; Malliakas, C. D.; Hauser, B. G.; Kanatzidis, M. G.; Nguyen, S. T.; Snurr, R. Q.; Hupp, J. T. *Nat. Chem.* **2010**, *2*, 944−948.
(28) Yazaydin, A. O.; Snurr, R. Q.; Park, T.-H.; Koh, K.; Liu, J.; LeVan, M. D.; Benin, A. I.; Jakubczak, P.; Lanuza, M.; Galloway, D. B.; Low, J. J.; Willis, R. R. *J. Am. Chem. Soc.* **2009**, *131*, 18198−18199.
(29) Keskin, S.; Sholl, D. S. *Langmuir* **2009**, *25*, 11786−11795.
(30) Valenzano, L.; Civalleri, B.; Sillar, K.; Sauer, J. *J. Phys. Chem. C* **2011**, *115*, 21777−21784.
(31) Wu, H.; Simmons, J. M.; Srinivas, G.; Zhou, W.; Yildirim, T. *J. Phys. Chem. Lett.* **2010**, *1*, 1946−1951.
(32) Hohenberg, P.; Kohn, W. *Phys. Rev. B* **1964**, *136*, B864−B871.
(33) Sun, Y. Y.; Kim, Y.-H.; Lee, K.; Zhang, S. B. *J. Chem. Phys.* **2008**, *129*, 154102.
(34) Chakarova-Käck, S. D.; Schröder, E.; Lundqvist, B. I.; Langreth, D. C. *Phys. Rev. Lett.* **2006**, *96*, 146107.
(35) Jeziorski, B.; Moszynski, R.; Szalewicz, K. *Chem. Rev.* **1994**, *94*, 1887−1930.
(36) Heelmann, A.; Jansen, G. *Phys. Chem. Chem. Phys.* **2003**, *5*, 5010−5014.
(37) Misquitta, A. J.; Jeziorski, B.; Szalewicz, K. *Phys. Rev. Lett.* **2003**, *91*, 033201-1−4.
(38) Osinga, V. P.; van Gisbergen, S. J. A.; Snijders, J. G.; Baerends, E. J. *J. Chem. Phys.* **1997**, *106*, 5091−5101.
(39) Tkatchenko, A.; Schefer, M. *Phys. Rev. Lett.* **2009**, *102*, 073005.
(40) Bludský, O.; Rubens, M.; Soldán, P.; Nachtigall, P. *J. Chem. Phys.* **2008**, *128*, 114102.
(41) Tkatchenko, A.; DiStasio, R. A.; Car, R.; Scheffler, M. *Phys. Rev. Lett.* **2012**, *108*, 236402-1−236402-5.
(42) Grimme, S. *J. Comput. Chem.* **2004**, *25*, 1463−1473.
(43) Grimme, S. *J. Comput. Chem.* **2006**, *27*, 1787−1799.
(44) Grimme, S.; Antony, J.; Ehrlich, S.; Krieg, H. *J. Chem. Phys.* **2010**, *132*, 154104-1−19.
(45) Dion, M.; Rydberg, H.; Schröder, E.; Langreth, D. C.; Lundqvist, B. I. *Phys. Rev. Lett.* **2004**, *92*, 246401-1−4.
(46) Bučko, T.; Hafner, J.; Lebègue, S.; Ángyán, J. G. *J. Phys. Chem. A* **2010**, *114*, 11814−11824.
(47) Atodiresei, N.; Caciuc, V.; Franke, J.-H.; Blügel, S. *Phys. Rev. B* **2008**, *78*, 045411.
(48) Kerber, T.; Sierka, M.; Sauer, J. *J. Comput. Chem.* **2008**, *29*, 2088−2097.
(49) Cooper, V. R. *Phys. Rev. B* **2010**, *81*, 161104(R).
(50) Román-Pérez, G.; Soler, J. M. *Phys. Rev. Lett.* **2009**, *103*, 096102-1−4.
(51) Jennes, G. R.; Karalti, O.; Al-Saiadi, W. A.; Jordan, K. D. *J. Phys. Chem. A* **2011**, *115*, 5955−5964.
(52) Wu, X.; Vargas, M. C.; Nayak, S.; Lotrich, V.; Scoles, G. *J. Chem. Phys.* **2001**, *115*, 8748−8757.
(53) Wu, Q.; Yang, W. *J. Chem. Phys.* **2002**, *116*, 515.
(54) Sun, X.; Yamauchi, Y. *J. Appl. Phys.* **2011**, *110*, 103701.
(55) Ziambaras, E.; Kleis, J.; Schröder, E.; Hyldgaard, P. *Phys. Rev. B* **2007**, *76*, 155425.
(56) Grimme, S.; Mück-Lichtenfeld, C.; Antony, J. *J. Phys. Chem. C* **2007**, *111*, 11199−11207.
(57) Cooper, V. R.; Kong, L.; Langreth, D. C. *Phys. Procedia* **2010**, *3*, 1417−1430.
(58) Jurečka, P.; Šponer, J.; Černý, J.; Hobza, P. *Phys. Chem. Chem. Phys.* **2006**, *8*, 1985−1993.
(59) Puzder, A.; Dion, M.; Langreth, D. C. *J. Chem. Phys.* **2006**, *124*, 164105.
(60) Li, S.; Cooper, V. R.; Thonhauser, T.; Puzder, A.; Langreth, D. C. *J. Phys. Chem A* **2008**, *112*, 9031.
(61) Cooper, V. R.; Thonhauser, T.; Puzder, A.; Schröder, E.; Lundqvist, B. I.; Langreth, D. C. *J. Am. Chem. Soc.* **2008**, *130*, 1304−1308.
(62) Cooper, V. R.; Thonhauserb, T.; Langreth, D. C. *J. Chem. Phys.* **2008**, *128*, 204102.
(63) Londero, E.; Schröder, E. *Phys. Rev. B* **2010**, *82*, 054116.
(64) Lee, K.; Kelkkanen, A. K.; Berland, K.; Andersson, S.; Langreth, D. C.; Schoder, E.; Lundqvist, B. I.; Hyldgaard, P. *Phys. Rev. B* **2011**, *84*, 193408.
(65) Kong, L.; Cooper, V. R.; Nijem, N.; Li, K.; Li, J.; Chabal, Y. J.; Langreth, D. C. *Phys. Rev. B* **2009**, *79*, 081407(R).
(66) Klimeš, J.; Bowler, D. R.; Michaelides. *J. Phys.: Condens. Matter* **2010**, *22*, 022201−5.
(67) Klimeš, J.; Bowler, D. R.; Michaelides. *Phys. Rev. B* **2011**, *83*, 195131.
(68) Lee, K.; Murray, E. D.; Kong, L.; Lundqvist, B. I.; Langreth, D. C. *Phys. Rev. B* **2010**, *82*, 081101.
(69) Dietzel, P. D. C.; Panella, B.; Hirscher, M.; Blom, R.; Fjellvg, H. *Chem. Commun.* **2006**, 959−961.
(70) Dietzel, P. D. C.; Morita, Y.; Blom, R.; Fjellvag, H. *Angew. Chem., Int. Ed.* **2005**, *44*, 6354−6358.
(71) Dietzel, P. D. C.; Blom, R.; Fjellvag, H. *Eur. J. Inorg. Chem.* **2008**, 3624−3632.
(72) Zhou, W.; Wu, H.; Yildirim, T. *J. Am. Chem. Soc.* **2008**, *130*, 15268−15269.
(73) Chui, S. S.-Y.; Lo, S. M.-F.; Charmant, J. P. H.; Orpen, A. G.; Williams, I. D. *Science* **1999**, *19*, 1148.
(74) Valenzano, L.; Civalleri, B.; Chavan, S.; Palomino, G. T.; Areań, C. O.; Bordiga, S. *J. Phys. Chem. C* **2010**, *114*, 11185−11191.
(75) Britt, D.; Furukawa, H.; Wang, B.; Glover, T. G.; Yaghi, M. *Proc. Natl. Acad. Sci. U.S.A.* **2009**, *106*, 20637−20640.
(76) Dietzel, P. D. C.; Besikiotis, V.; Blom, R. *J. Mater. Chem.* **2009**, *19*, 7362−7370.
(77) Bao, Z.; Yu, L.; Ren, Q.; Lu, X.; Deng, S. *J. Colloid Interface Sci.* **2011**, *353*, 549−556.
(78) Liu, J. Ph.D. Dissertation, Vanderbilt University, May 2011.
(79) Dietzel, P. D. C.; Johnsen, R. E.; Fjellvåg, H.; Bordiga, S.; Groppo, E.; Chavanc, S.; Blom, R. *Chem. Commun.* **2008**, *2*, 5125−5127.
(80) Wang, Q. M.; Shen, D.; Bülow, M.; Lau, M. L.; Deng, S.; Fitch, F. R.; Lemcof, N. O.; Semanscin, J. *Microporous Mesoporous Mater.* **2002**, *55*, 217−230.
(81) Liang, Z.; Marshall, M.; Chaffee, A. L. *Energy Fuels* **2009**, *23*, 2785−2789.
(82) Farrusseng, D.; Daniel, C.; Gaudillère, C.; Ravon, U.; Schuurman, Y.; Mirodatos, C.; Dubbeldam, D.; Frost, H.; Snurr, R. Q. *Langmuir* **2009**, *25*, 7383−7388.
(83) Poloni, R.; Smit, B.; Neaton, J. B. *J. Phys. Chem. A* **2012**, *116*, 4957−4964.
(84) Adamo, C.; Barone, V. *J. Chem. Phys.* **1999**, *110*, 6158−6170.
(85) Perdew, J. P.; Burke, K.; Ernzerhof, M. Generalized Gradient Approximation Made Simple. *Phys. Rev. Lett.* **1996**, *77*, 3865−3868.
(86) Bohm, D.; Pines, D. *Phys. Rev.* **1953**, *92*, 609−625. Langreth, D. C.; Perdew, J. P. *Phys. Rev. B* **1977**, *15*, 2884−2901.
(87) Kresse, G.; Hafner, J. *Phys. Rev. B* **1993**, *47*, 558−561. Kresse, G.; Furthmüller, J. *Phys. Rev. B* **1996**, *54*, 11169−11186.
(88) Blöchl, P. E. *Phys. Rev. B* **1994**, *50*, 17953−17979. Kresse, G.; Joubert, D. *Phys. Rev. B* **1999**, *59*, 1758−1775.
(89) Vosko, S. H.; Wilk, L.; Nursair, M. *Can. J. Phys.* **1980**, *58*, 1200−1211.
(90) Perdew, J. P.; Wang, Y. *Phys. Rev. B* **1986**, *33*, 8800−8802.
(91) Murray, E. D.; Lee, K.; Langreth, D. C. *J. Chem. Theory Comput.* **2009**, *5*, 2754−2762.
(92) Hertzberg, G. *Infrared and Raman Spectra*; van Nostrand Reinhold: New York, 1945.
(93) Queen, W. L.; Brown, C. M.; Britt, D. K.; Zajdel, P.; Hudson, M. R.; Yaghi, O. M. *J. Phys. Chem. C* **2011**, *115*, 24915−24919.
(94) Wallace, D. C. *Thermodynamics of Crystals*; John Wiley & Sons: New York, 1972.

(95) Rickman, J. M.; LeSar, R. *Annu. Rev. Mater. Res.* **2002**, *32*, 195−217.
(96) Wei, S.; Chou, M. Y. *Phys. Rev. Lett.* **1992**, *69*, 2799−2802.
(97) Aprea, P.; Caputo, D.; Gargiulo, N.; Iucolano, F.; Pepe, F. *J. Chem. Eng. Data* **2010**, *55*, 3655−3661.
(98) Moellmer, J.; Moeller, A.; Dreisbach, F.; Glaeser, R.; Staudt, R. *Microporous Mesoporous Mater.* **2011**, *138*, 140−148.
(99) Byrd, E. F. C.; Scuseria, G. E.; Chabalowski, C. F. *J. Phys. Chem. B* **2004**, *108*, 13100−13106.
(100) Qiu, L.; Xiao, H. M.; Zhu, W. H.; Xiao, J. J.; Zhu, W. *J. Phys. Chem. B* **2006**, *110*, 10651−10661.
(101) Byrd, E. F. C.; Rice, B. M. *J. Phys. Chem. C* **2007**, *111*, 2787−2796.
(102) Conroy, M. W.; Oleynik, I. I.; Zybin, S. V.; White, C. T. *Phys. Rev. B* **2008**, *77*, 094107-1−8.
(103) Zhang, X. X.; Chui, S. S.-Y.; Williams, I. D. *J. Appl. Phys.* **2000**, *87*, 6007.
(104) Grajciar, L.; Wiersum, A. D.; Llewellyn, P. L.; Chang, J.-S.; Nachtigall, P. *J. Phys. Chem. C* **2011**, *115*, 17925−17933.